Research Square

Preprints are preliminary reports that have not undergone peer review.
They should not be considered conclusive, used to inform clinical practice,
or referenced by the media as validated information.

# Drop sloshing on vibrating compliant substrates

**MD Emazuddin Alif**
University of Tennessee at Knoxville
**Ahmad Naseri Karimvand**
University of Tennessee at Knoxville
**Jeffrey Lynn Kauffman**
University of Central Florida
**Andrew Keith Dickerson**
ad@utk.edu

University of Tennessee at Knoxville

**Research Article**

**Keywords:**

**Posted Date:** August 12th, 2026

**DOI:** https://doi.org/10.21203/rs.3.rs-10619269/v1

**License:** This work is licensed under a Creative Commons Attribution 4.0 International License.
Read Full License

**Additional Declarations:** No competing interests reported.

# Drop sloshing on vibrating compliant substrates

Md Emazuddin Alif[1a], Ahmad Naseri Karimvand[1b],
Jeffrey L. Kauffman[2c], Andrew K. Dickerson[1d*]
[1]Mechanical and Aerospace Engineering, University of Tennessee, Knoxville
[2]Mechanical and Aerospace Engineering, University of Central Florida, Orlando
* Corresponding author: ad@utk.edu
ORCID: [a]0000-0001-5708-475X, [b]0009-0005-3429-9471, [c]0000-0003-1980-9865, [d]0000-0003-1220-1048

**Abstract**

This study aims to shed light on the complex physics at the interface of sloshing, sessile drops, and compliant, dynamic surfaces, a problem that has seemingly infinite permutations. We do so through experiment and modeling to establish mathematical and analytical approaches for deformable, two-phase systems. Such systems are relevant for surface decontamination and engineered systems where drop control is paramount. We characterize the vibratory responses of 5-$\mu$L water drops on elastic substrates, inspired by the pre-flight wing fluttering routine employed by insects for dewetting. We vibrate cantilevers constructed from hydrophilic Kapton and hydrophobic polytetrafluoroethylene (PTFE) vertically using an electrodynamic shaker and conduct high-speed videography of the interactions between the deforming drops and the substrate. The natural frequency of the drop-cantilever system is lower than that of the individual drop on a similar rigid surface and a free beam of the same material, showing that liquid drops dominate the natural frequency of the system. For a freely vibrating system, the drop deformation and cantilever vibration are always at the same frequency. We define drop 'sloshiness' as the normalized area change from the sessile shape of two orthogonal projections of the drop. Drop deformation heatmaps generated from temporal deformation of drops reveal that pinned drops prefer 'jetting' mode, whereas drops with moving contact lines promote 'spreading mode'. Overall sloshiness values are similar for both pinned and unpinned contact lines. Sloshiness scales well with the Womersley number for both PTFE and Kapton beams.

## 1 Introduction

The need to decontaminate remote surfaces presents challenges when such structures are at the similar scales to their contaminants. In the absence of deliberate decontamination systems, excitation of surfaces provides a means by which they may self-clean or dry. In this study, we further explore the behavior of surface-contaminating sessile water drops of vibrating, elastic surfaces for the purposes of understanding the requirements of drop removal by such a surface. Our experimental system, an elastomeric cantilever affixed to a rapidly translating post, presents a coupled system in which the sloshing and elastic surface dynamics are influenced by each other. By imposing a variety of base vibration conditions, we can elicit different sloshing behaviors from a drop placed near the cantilever tip, as shown in **Fig.1**.

Traditional research on drop-cantilever interactions, for fibers and beams, has focused on one-dimensional motion from drops impacting the cantilever, vibration, and ejection[1–17]. The ejection of drops from surfaces, while far from unstudied, has received less attention and is arguably more complex because of the strong temporal component of surface vibration. Drop ejection studies have focused on one-dimensional surface motion deforming[18–22] and shattering[14,23] drops, sliding induced by wind shear[15,24] or body forces[25], and vibration in the fixed end of the cantilever[8]. Large drops with a contact diameter greater than 10 mm are vulnerable to removal by gravity, but drops smaller than the capillary length (2.7 mm for water) are harder to displace. Drop movement presupposes overcoming contact angle hysteresis[19,21], and in instances where the drop is not immediately provided an acceleration sufficient for ejection, it will slosh. Drop oscillations on a vertical surface parallel to gravity are in competition with contact angle hysteresis, introducing a ratcheting downward motion[20]. Optical deflection techniques used on sessile drops disturbed by an impulse reveal that the dominant source of damping on sessile liquid drops is due to bulk viscosity, with contact line

dissipation becoming more relevant in smaller contact angles[15]. A closer look at the shape oscillations of sessile drops excited by a speaker exhibits pinned and de-pinned contact lines at lower and higher amplitude vibrations, respectively. Pinned contact lines result in symmetric shape oscillation modes similar to harmonic standing waves, whereas oscillations for mobile contact lines are more irregular[26]. Individual modes for both instances of pinned and unpinned contact lines have corresponding resonant frequencies[22]. The lobe size of drops increases dramatically when excitation frequency reaches resonance[13]. More recent studies have focused on sessile drops damping the vibration of the substrate structures. Sessile drops deposited at the free end of a cantilever beam damp motion when an initial deflection is applied[7], behaving similarly as a particle impact damper (PID). However, unlike PIDs, drops do not have a lower acceleration threshold in which their ability to damp ceases. The most or least viscous drops do not correspond to maximum damping; an intermediate viscosity provides the most effective balance between sloshing and internal dissipative energy[7].

The dynamics of sessile drops on rigid substrates are well characterized theoretically. The natural frequencies and mode shapes of sessile drops can be understood as constrained analogs of the classical Rayleigh–Lamb spectrum for free spherical drops, with the substrate modifying the spectral ordering depending on the equilibrium contact angle and the contact-line boundary condition[27,28]. Bostwick & Steen (2014)[28] developed an inviscid theory for sessile drop oscillations that yields the frequency spectrum as a function of contact angle for pinned, free (constant contact angle), and dynamic (Hocking) contact-line conditions, classifying modes by polar and azimuthal wavenumbers $[k, l]$ into zonal ($l = 0$), sectoral ($k = l$), and tesseral ($k > l$) families. These theoretical predictions have been validated experimentally[29] and extended to include the effects of contact-line dissipation under forced oscillation[30], pressure modes[31], and gravitational effects[32]. A comprehensive review of the stability of constrained capillary surfaces, including sessile drops, is given by Bostwick & Steen (2015)[33], and a unifying classification of droplet motions into a "periodic table" of modes has been proposed[34]. Drop oscillations on vertically vibrated rigid substrates have also been studied experimentally, with resonant and rolling behaviors observed for millimetric drops[35].

While these foundational works establish a thorough understanding of sessile drop oscillations on rigid substrates, the coupled dynamics of a sloshing drop on a vibrating elastic substrate remain largely unexplored. In the present system, the substrate is itself compliant and vibrating as a cantilever beam, introducing a coupling between solid and liquid dynamics that is not captured by existing inviscid eigenvalue theories. Furthermore, the forced vibration of the cantilever base imposes sustained oscillations rather than the impulse response or parametric excitation considered in most prior work. Our study addresses this gap and introduces a global deformation metric, sloshiness $\mathcal{S}$, that complements modal decomposition with a spatial measure of drop deformation obtained from two orthogonal high-speed imaging projections. In this study, we force flexible polytetrafluoroethylene (PTFE) and Kapton cantilever beams at their fixed end over a range of frequencies and amplitudes, and observe the drop response at the free end using high-speed videography, as shown in **Fig.1**. Drop deformation depends on cantilever stiffness and contact angle of the surface, as seen in **Fig.1**a-c for Kapton and **Fig.1**d-f for PTFE. Based on the time in the vibration cycle, the liquid drop can be either in jetting (**Fig.1**b,e) or spreading (**Fig.1**c,f) mode. We propose a novel term, sloshiness $\mathcal{S}$, to represent how much a liquid drop has deformed or sloshed from its initial state. Further description of $\mathcal{S}$ is given in Section 3.2.

# 2 Methods

We manufacture our elastic cantilever beams by cutting 3.6 mm × 10 mm rectangles out of 0.003-inch thick Kapton sheets and 0.005-inch thick polytetrafluoroethylene (PTFE) sheets with a SH-G570 USB6N57-60W laser cutter. Each beam is affixed to the top of a rigid post on a The Modal Shop Inc. K2007E01 electrodynamic shaker. A sine wave produced by a Koolerton DDS Signal Generator/Counter informs the motion of the shaker post. We produce 5$\mu$L water drops with a Carolina Scientific micropipetter and place them on the tip of the beam, as shown in **Fig.1**.

For the first phase of the experiment, we place the liquid drops on flexible Kapton and PTFE beams and provide the free end of the cantilever with a small initial displacement. We perform FFT on the temporal deflection of the beam to obtain its natural frequency, and fit the beam response to an exponentially decaying cosine wave to find the beam damping coefficients, details of which are provided in Section 3.1. The first natural frequency of the drop-Kapton cantilever system is measured to be $f_{\mathrm{Kap}} = 90$ Hz, and

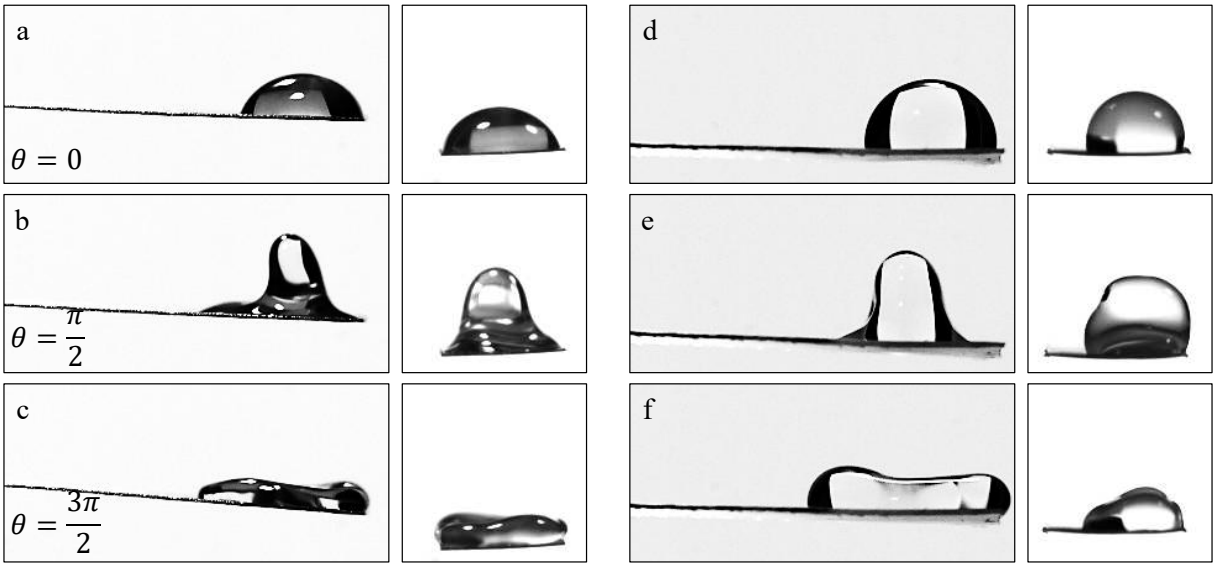



**Figure 1:** Drop deformation modes for Kapton (left) and PTFE (right) beams. **(a)**, **(d)** Initial drop shape. **(b)**, **(e)** Jetting deformation mode. **(c)**, **(f)** Spreading deformation mode.

the drop-PTFE cantilever system to be $f_{\text{Tef}} = 82$ Hz. For the next phase of the study, we conduct our experiments centering around the natural frequencies of both systems at 80, 90, 100, and 110 Hz, and away from resonance at 140 Hz, increasing the amplitudes until liquid ejects for each frequency values. We wait until the drop-cantilever system has reached steady state before recording. We record each trial at 12,000 fps with a Photron Nova S6 fitted with a SIGMA 105mm 1:2.8 DG Macro HSM lens. Zoom levels permit resolutions ranging from $0.019-0.035$ mm/pixel. Neewar NL-288A RC LED light panel provides backlighting for repeatable binarization in MATLAB. We track post and beam positions, drop height and spread, and measure dynamic quantities within binarized videos using bespoke code. We produce at least three replicates of each experimental condition. A schematic of the experimental setup is provided in **Fig.2**.

# 3 Results

## 3.1 Liquid drops dominate natural frequency of the drop-cantilever system

While the dynamics of cantilever beams with non-negligible solid masses on the tip have been thoroughly explored[36–38], substituting a liquid drop for a point mass or particle damper presents cases that have not been modeled, to our knowledge. The propensity of a liquid drop to slosh introduces coupled dynamics between the drop and the cantilever, where the cantilever deflection depends on the sloshing of the drop, and the drop deformation is dependent on the motion of the cantilever. In order to better our understanding of this co-dependency, we begin with an experiment to determine the dynamic properties of the drop-surface, the cantilever, and the drop-cantilever systems, separately, and without base vibration.

We place 5-$\mu$L liquid drops on rigid Kapton and PTFE surfaces with $\theta_{\text{e,Kap}} \simeq 60 - 70^\circ$ and $\theta_{\text{e,PTFE}} \simeq 100 - 110^\circ$, respectively. We assume the drop is axisymmetric, and the surface is ideal, free of blemishes or contaminants. We disturb the drop with an impulsively provided displacement of the riged base, vertically, and record the drop aspect ratio $h/d$, where $h$ is the height of the drop from the surface and $d$ is the diameter of the contact patch. FFT performed on the temporal aspect ratio of the drop provides the natural frequencies for our drops atop Kapton and PTFE surfaces, $f_{\text{n,drop}} = 111.7,\ 90.7$ Hz ($N = 6,\ 5$; $s = 3.9,\ 4.2$), respectively. A plot of a representative temporal aspect ratio $h/d$ and its FFT is shown in **Fig.3**a-b.

These measured natural frequencies can be compared with predictions from the inviscid theory of Bostwick & Steen (2014)[28], which provides the oscillation frequency spectrum for sessile drops as a function of contact

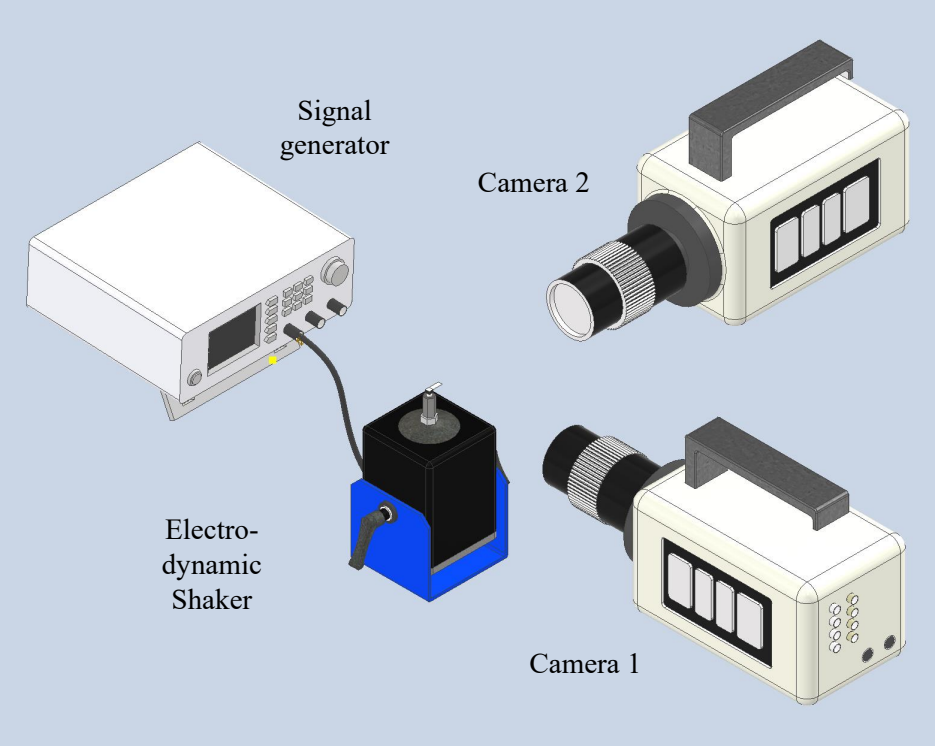



**Figure 2:** Schematic of the experimental setup.

angle and contact-line condition. For our Kapton surfaces ($\theta_e \simeq 60$–$70°$), the observed $f_{n,drop} = 111.7$ Hz is consistent with the lowest axisymmetric (zonal $[2,0]$) mode with a pinned contact line[28,29]. For PTFE ($\theta_e \simeq 100$–$110°$), the inviscid theory of Bostwick & Steen predicts that the frequency of this same $[2,0]$ mode decreases with increasing contact angle[28]; our lower measured $f_{n,drop} = 90.7$ Hz on the more hydrophobic PTFE follows this trend and is consistent with the contact-angle dependence of the Rayleigh spectrum as modified by a constraining substrate[27,29]. The aspect-ratio oscillation we track ($h/d$) is an axisymmetric observable and thus most sensitive to the $[k,0]$ zonal mode family.

We perform a pluck test on our Kapton and PTFE beams and track the free end of the beam with high-speed cameras during ring-down. The natural frequencies of the Kapton and PTFE cantilevers extracted from an FFT of temporal tip displacement are $f_{n,\,beam} = 221.6,\ 135.9$ Hz ($N = 3,\ 3$; $s = 0.2,\ 1.0$), respectively. The ring-down deflection and its FFT for a representative trial are shown in **Fig.3**c and d. We repeat the same experiment with a liquid drop at the end of the cantilever. The allowable beam deflection for this case is greatly reduced to avoid drop ejection from the beam. We observe that the drop deformation and beam deflection oscillate in same frequency for the entire period for both beam materials. The natural frequencies of the combined system are found to be $f_{n,sys} = 89.5,\ 81.8$ Hz ($N = 6,\ 4$; $s = 2.3,\ 2.8$), respectively. Time-series data and their FFTs for the combined system are shown in **Fig.3**e, f, g, and h.

The coupled system frequencies ($f_{n,sys} = 89.5$ and $81.8$ Hz) are substantially lower than either the uncoupled drop or beam natural frequencies, a result consistent with the added-mass effect of a liquid load on a vibrating structure[7,16]. This frequency reduction exceeds what would be predicted by simply adding a rigid point mass equal to the drop mass at the cantilever tip[36,38], indicating that the sloshing degree of freedom of the drop participates in the coupled dynamics and to lower the system frequency[11,16]. Such behavior is analogous to the frequency shifts observed when substrate constraints modify the Rayleigh spectrum of sessile drops[27].

The plucked drop-on-beam systems behave as underdamped harmonic oscillators. We fit their temporal deflection $y$ with the analytical solution of a second-order equation of motion for a harmonic oscillator,

$$y = e^{-\lambda t} a \cos\left(2\pi f_{n,sys} t + \phi\right), \tag{1}$$

where $\phi$ is the phase shift, $a$ is the initial deflection, and $\lambda$ is the decay rate. Oscillation decay rate is a function of the damping coefficient of the system, $c$, and the effective mass of the system $m_{\text{eff}}$,

$$\lambda = c/2m_{\text{eff}}. \tag{2}$$

The effective mass of a cantilever beam of non-negligible mass, if concentrated at a point on the beam tip, is represented by[16] $m_{\text{eff}} = 0.24273\ m_{beam}$. For our experiments, $m_{\text{eff}}$ for Kapton and PTFE are 0.773 mg and 2.54 mg respectively. Therefore, from Eq.(2), we find the beam damping coefficient to be $c = 3.79 \times 10^{-5},\ 2.67 \times 10^{-4}$ N $\cdot$ s/m for Kapton and PTFE, respectively. The decay rate $\lambda$ and damped natural frequency $f_{\text{n,sys}}$ are used to calculate a spring constant,

$$k = m_{\text{eff}}[(2\pi f_n)^2 - \lambda^2]. \tag{3}$$

Our Kapton and PTFE beams have $k = 1.38,\ 1.70$ N/m respectively.

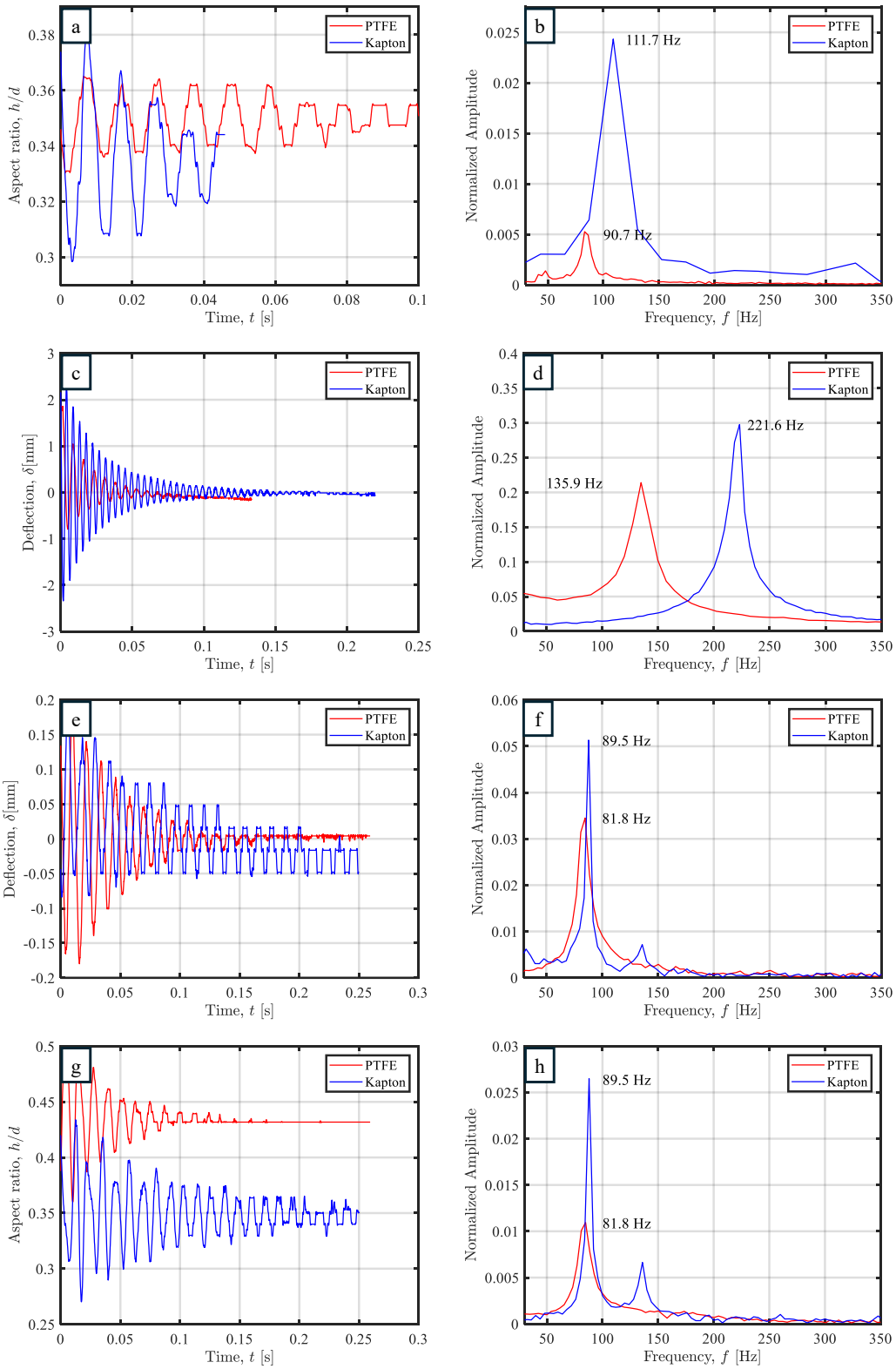



**Figure 3:** System response to initial perturbation condition. Aspect ratio, $h/d$ versus time, $t$ for liquid drop on **(a)** rigid Kapton and PTFE surface, and **(g)** flexible Kapton and PTFE beams and their respective FFTs ((**b**), (**h**)). Cantilever deflection, $\delta$ vs time, $t$ for **(c)** only cantilever beam and **(e)** cantilever beam with liquid drop at the end, and their respective FFTs ((**d**), (**f**)). For drop-cantilever systems, the liquid drop oscillates at the same frequency as the cantilever deflection.

### 3.2 Drop sloshing scales with Womersley number

With natural frequencies for ring-down vibration in hand and guiding selection for forced vibration frequencies, we turn our attention to drop sloshing when the cantilever is exciting by sinusoidal vertical translation of the base. We decompose liquid drop deformation into two modes, 'jetting' and 'spreading', as shown in **Fig.1**c,f. The jetting mode exists when the drop dome is higher than the initial dome height, and the spreading mode when the drop is wider than the initial width, even if the drop contact line is pinned. The deformation mode of a drop at any time can be any combination of its jetting and spreading mode. We quantify the jetting and spreading modes of the drop from two orthogonal views obtained as shown in **Fig.2**. We propose 'sloshiness' $\mathcal{S}$ as a numerical value that represents the extent of deformation, or sloshing, from its initial state. We express the two orthogonal frames of a trial at time $t$ by the binary matrices $F_x$ and $F_y$, with their initial frames being $F_x(0)$ and $F_y(0)$ respectively. Each frame $F$ is centered around the midpoint of the contact line between the droplet and the surface. Therefore, sloshiness is defined by,

$$\mathcal{S}(t) = \frac{a^2 \sum_i \sum_j |F_x(t)_{i,j} - F_x(0)_{i,j}| + b^2 \sum_i \sum_j |F_y(t)_{i,j} - F_y(0)_{i,j}|}{a^2 \sum_i \sum_j F_x(0)_{i,j} + b^2 \sum_i \sum_j F_y(0)_{i,j}}, \tag{4}$$

where $a$ and $b$ are pixel-to-length conversion factor for each orthogonal view. Each element of the matrices $F_{x,0}$ and $F_{y,0}$ corresponds to individual pixels that have a dimension of area, so sloshiness, $\mathcal{S}$ is a measure of normalized change in area of the projection of the liquid drop with respect to its initial area. For a rigid undeforming mass, $\mathcal{S}$ will always be zero, whereas for a sloshing mass $\mathcal{S}$ is a nonzero quantity. Please note that measurement of $\mathcal{S}$ requires the presence of a contact line between the droplet and the surface; our definition of $\mathcal{S}$ breaks down when the mass is ejected from the surface.

We can visualize $\mathcal{S}$ by looking at liquid drop heatmaps with subtracted initial area, as shown in **Fig.4**a. More intense tones represent more repeated motion over the course of a trial. Warmer colors correspond to the drop portion protruding out of the initial projection, while cooler colors denote drops collapsing within the initial projection. Color gradient from the subtracted initial projection also shows whether the contact line remains pinned. Temporal sloshiness of the representative trial in **Fig.4**a is shown in **Fig.4**b.

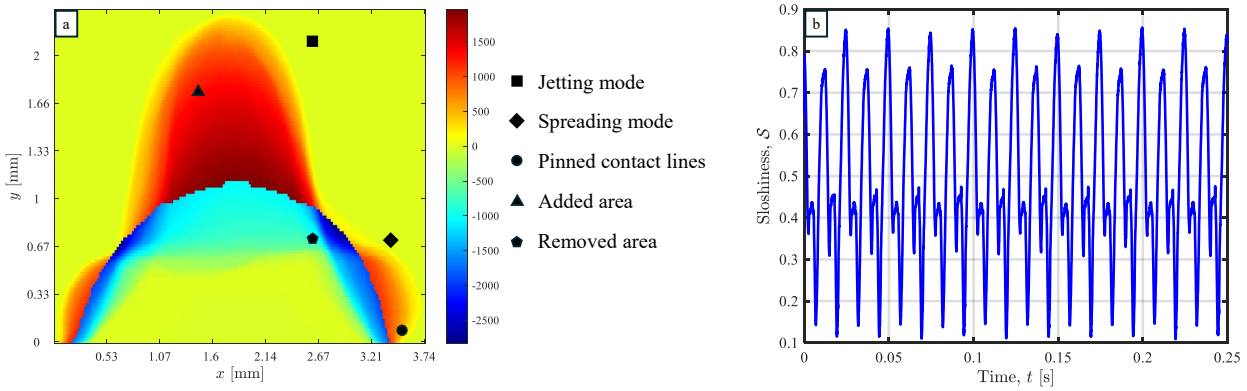



**Figure 4:** Sloshiness, $\mathcal{S}$ of a sessile droplet vibrating on a Kapton beam driven at 80 Hz. **(a)** Drop heatmap with subtracted initial area. Warmer colors represent additional drop area protruding outward from the initial drop projection, whereas cooler tones present areas removed from the initial projection due to droplet collapsing on itself. **(b)** Temporal sloshiness, $\mathcal{S}(t)$ vs time, $t$ [s].

Sloshiness $\mathcal{S}$ as defined is a visual parameter calculated from images. We desire a physics-informed analog by which to compare $\mathcal{S}$. Drop shapes while sloshing depend on the liquid viscosity that damps the drop bulk motion, and the surface tension resisting the stretching of the drop boundary. These two fluid parameters provide a resistive force proportional to the velocity and displacement within the drop continuum. Prior work on drops impacting on cantilevered substrates have modeled drop cantilever systems as two mass-spring-dampers[16]. We too model a drop-cantilever-base system as two-mass-spring-dampers on a moving base, as seen in **Fig.5**, such that the motion of the free end of the cantilever and that of the centroid of the

liquid drop are represented by two rigid point masses. As a liquid droplet sloshes more, the displacement of the drop centroid would be higher, whereas a less sloshing superstrate would have more limited centroid movement. Therefore, in order to predict how liquid drops might slosh in response to external input in our system, we can consider the point mass representation of the drop centroid as a physical analog to sloshiness.

We note that this two-degree-of-freedom (2-DOF) model is a reduced-order engineering approximation, not a complete description of sessile drop dynamics. The full theoretical framework developed by Bostwick & Steen[28] yields a spectral eigenvalue problem whose solutions describe the complete set of oscillation modes $[k, l]$ with their associated frequencies and mode shapes. Our lumped-parameter approach does not resolve these individual modes, but rather treats the drop as a point mass whose centroid displacement serves as a proxy for the lowest-order deformation. This reduced-order strategy is appropriate for our coupled drop-cantilever system, where the primary objective is to predict how base excitation amplitude and frequency affect overall drop deformation, and is consistent with the lumped-parameter models used in prior drop-cantilever studies[16,39].

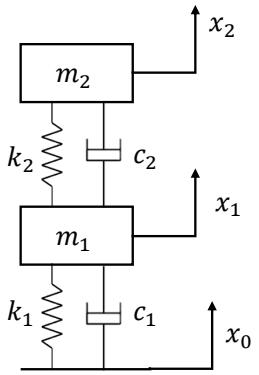



**Figure 5:** Math model of cantilever beam and drop.

Let the effective mass of the cantilever beam be modeled as a point mass $m_1$, and the effective mass of the drop be a point mass $m_2$. We model the cantilever beam and the liquid drop atop as two different mass-spring-damper systems, where their spring coefficients and damping coefficients are $k_1$, $k_2$, and $c_1$, $c_2$, respectively. The displacement of the base is $x_0$, and the absolute displacement of each mass is $x_1$ and $x_2$, respectively. The spring constant $k_2$ represents the capillary restoring force that resists drop deformation, while the damping coefficient $c_2$ encompasses both bulk viscous dissipation and contact-line dissipation[30]. The relative magnitudes of these two dissipation mechanisms depend on contact angle and contact-line mobility[15,30]. The equations of motion of the two masses are as follows:

$$m_1\ddot{x_1} + (c_1 + c_2)\dot{x_1} - c_2\dot{x_2} + (k_1 + k_2)x_1 - k_2x_2 = c_1\dot{x_0} + k_1x_0, \tag{5}$$

$$m_2\ddot{x_2} - c_2\dot{x_1} + c_2\dot{x_2} - k_2x_1 + k_2x_2 = 0. \tag{6}$$

We define $z_1 = x_1 - x_0$ and $z_2 = x_2 - x_1$. Swapping in the relative terms for the absolute terms in Eq.(5) and Eq.(6), we get:

$$\begin{bmatrix} m_1 & 0 \\ m_2 & m_2 \end{bmatrix} \begin{Bmatrix} \ddot{z}_1 \\ \ddot{z}_2 \end{Bmatrix} + \begin{bmatrix} c_1 & -c_2 \\ 0 & c_2 \end{bmatrix} \begin{Bmatrix} \dot{z}_1 \\ \dot{z}_2 \end{Bmatrix} + \begin{bmatrix} k_1 & -k_2 \\ 0 & k_2 \end{bmatrix} \begin{Bmatrix} z_1 \\ z_2 \end{Bmatrix} = \begin{Bmatrix} -m_1\ddot{x} \\ -m_2\ddot{x} \end{Bmatrix} \tag{7}$$

Converting to matrix notation,

$$M\ddot{Z} + C\dot{Z} + KZ = U(t), \tag{8}$$

where

$$M = \begin{bmatrix} m_1 & 0 \\ m_2 & m_2 \end{bmatrix}, \quad C = \begin{bmatrix} c_1 & -c_2 \\ 0 & c_2 \end{bmatrix}, \quad K = \begin{bmatrix} k_1 & -k_2 \\ 0 & k_2 \end{bmatrix}, \quad Z = \begin{Bmatrix} z_1 \\ z_2 \end{Bmatrix}, \quad U(t) = \begin{Bmatrix} -m_1 \\ -m_2 \end{Bmatrix} \ddot{x}(t).$$

The relative displacement notation in Eq.(8) introduces the effects of base acceleration into the equation, akin to the inertial forces experienced by a passenger due to sudden movement of a vehicle.

In our experiments the base excitation is harmonic, therefore the input acceleration is a pure cosine wave, $\ddot{x}(t) = A_0 \cos(\omega t)$, where $A_0 = -\omega^2 a_0$ is the amplitude of acceleration, $a_0$ is the amplitude of displacement, and $\omega$ is the driving frequency. Therefore, the input forcing function becomes,

$$U(t) = \begin{Bmatrix} -m_1 A_0 \\ -m_2 A_0 \end{Bmatrix} e^{i\omega t} = U_0 e^{i\omega t} \tag{9}$$

The analytical solution to Eq.(7) with a harmonic input has a transient and a steady-state response. In our study, we focus on the steady-state response of the experimental system, many cycles after the initiation of base vibration. At steady state, the displacements of the masses take the same harmonic form,

$$Z(t) = \begin{Bmatrix} Z_{1,s} \\ Z_{2,s} \end{Bmatrix} e^{i\omega t} = Z_s e^{i\omega t}, \quad \dot{Z}(t) = i\omega Z_s e^{i\omega t}, \quad \ddot{Z}(t) = -\omega^2 Z_s e^{i\omega t}. \tag{10}$$

Here $Z_s$ is a vector of complex amplitude, encoding both physical displacement and phase shift information of the masses. Substituting Eq.(10) into Eq.(8),

$$[-\omega^2 M + i\omega C + K] Z_s = U_0. \tag{11}$$

Plugging in the matrices for $M$, $C$ and $K$ from Eq.(7),

$$D(\omega) = \begin{bmatrix} (k_1 - m_1\omega^2 + ic_1\omega) & (-k_2 - ic_2\omega) \\ (-m_2\omega^2) & (k_2 - m_2\omega^2 + ic_2\omega) \end{bmatrix}. \tag{12}$$

Here $D(\omega)$ is the frequency-dependent coefficient matrix, often called the dynamic stiffness matrix in structural dynamics, that governs the steady-state frequency response of the coupled system. Therefore, the analytical solution becomes

$$Z_s = D(\omega)^{-1} U_0, \tag{13}$$

or,

$$Z_s = \frac{1}{\det(D)} \begin{bmatrix} (k_2 - m_2\omega^2 + ic_2\omega) & (k_2 + ic_2\omega) \\ (m_2\omega^2) & (k_1 - m_1\omega^2 + ic_1\omega) \end{bmatrix} \begin{Bmatrix} -m_1 A_0 \\ -m_2 A_0 \end{Bmatrix}. \tag{14}$$

The terms in the coefficient matrices are constant. Therefore, we see that the magnitude of steady-state displacement of the masses, specifically the drop centroid ($Z_{2,s}$), is proportional to the displacement of the base. The solution to Eq.(14) requires knowledge of $k_1$, $k_2$, $c_1$, and $c_2$ for the beam and sloshing drops, and assumes these are constant. Such a retrieval of these values for a drop is an area for future research. Instead, we use the insights Eq.(14) provides on acceleration to seek a dimensionless group that relates $\mathcal{S}$ to base acceleration.

The Womersley number $\alpha = L(2\pi f \rho/\mu)^{1/2}$ captures the ratio of oscillatory inertia to viscous effects and naturally incorporates both the amplitude and frequency of excitation, and $\alpha$ collapses our data well across all tested frequencies, as shown in Figs. 6 and 7. We note that the Womersley number is not the conventional dimensionless group used in sessile drop oscillation studies, but our use here is not the first[8]. A vibration Bond number $\mathrm{Bo}_v = \rho A \omega^2 R^2/\sigma$, which compares inertial acceleration to capillary restoring pressure, is more common in that literature[28,29]. However, in our coupled system the relevant driving parameter is the base

acceleration amplitude $A_0 = \omega^2 a_0$, and the drop response depends on both viscous damping and capillary restoring forces.

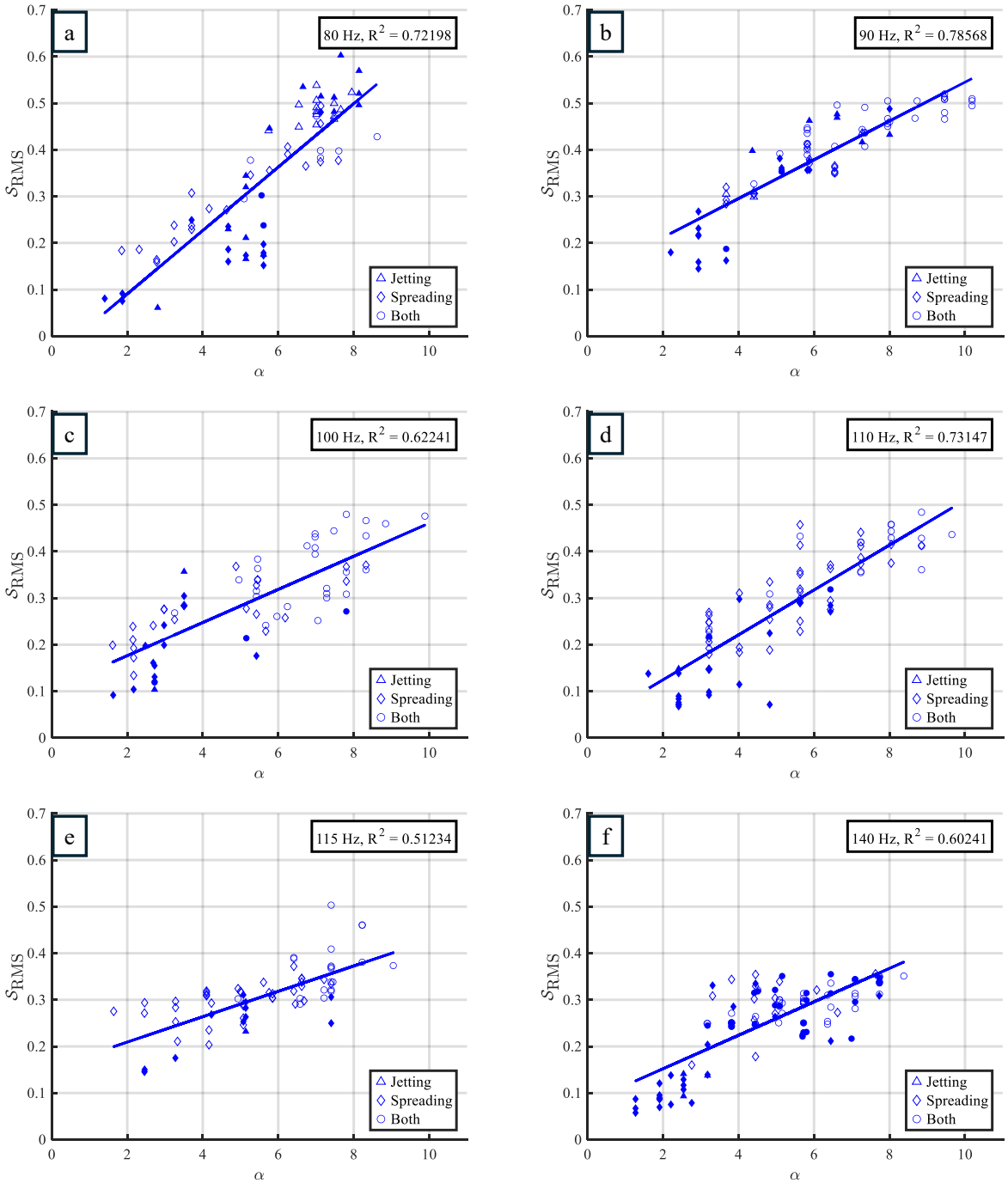



**Figure 6:** Sloshiness, $\mathcal{S}_{\mathrm{RMS}}$ vs $\alpha$ for a Kapton beam driven at various frequencies. Filled markers correspond to pinned contact lines.

We choose the Womersley number, $\alpha = L(2\pi f \rho/\mu)^{1/2}$, where $f$ is shaker frequency, $L$ is shaker amplitude, $\rho = 1000$ kg/m$^3$ is the density of water, and $\mu = 1.002 \times 10^{-3}$ Pa·s is the dynamic viscosity of water. While the Womersley number is typically used for pulsatile flows, we use it here to describe the oscillatory sloshing

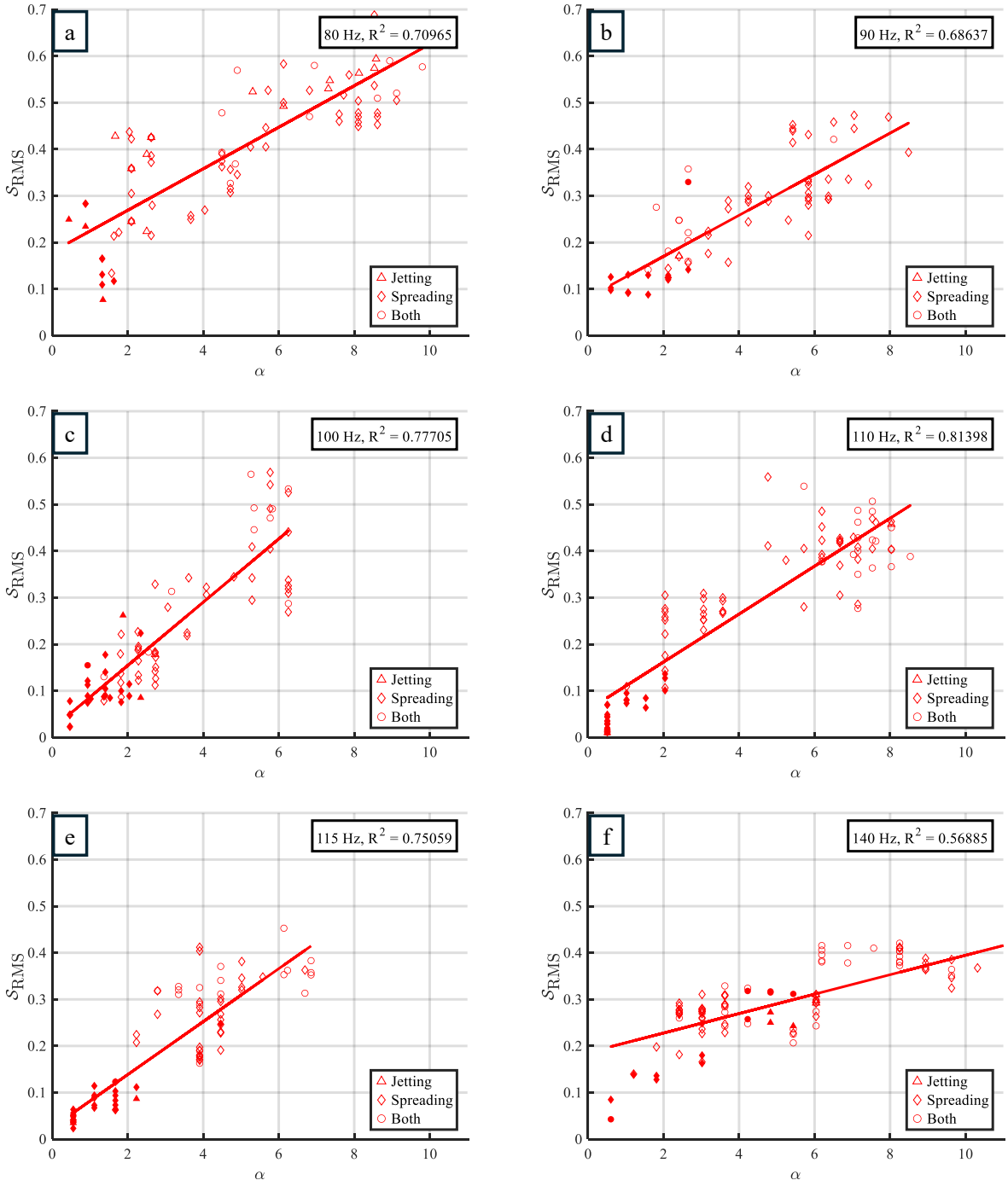



**Figure 7:** Sloshiness, $\mathcal{S}_{\mathrm{RMS}}$ vs $\alpha$ for a PTFE beam driven at various frequencies. Filled markers correspond to pinned contact lines.

of our drops. The acceleration of the base is a function of its frequency and amplitude of vibration, both of which appear in $\alpha$. As both base acceleration and $\alpha$ depend linearly on the amplitude of base displacement, at a constant frequency, the centroid displacement scales identically with both parameters. Since we consider

centroid motion as a physical analog of sloshiness, we can expect,

$$\mathcal{S} \sim \alpha. \tag{15}$$

Considering that sloshiness is temporal and multi-modal (**Fig.4**b), we cannot express a singular representative value for each trial from solely the amplitude of temporal $\mathcal{S}$. So, we take the root mean square (RMS) of the temporal $\mathcal{S}$. We plot $\mathcal{S}_{\mathrm{RMS}}$ against $\alpha$ in **Fig.6** and **Fig.7** for Kapton and PTFE respectively for $f = 80,\ 90,\ 100,\ 110,\ 115$ and 140 Hz. Our choice of shaker frequency is informed by the natural frequencies $f_{\mathrm{n,sys}}$ of the drop-cantilever systems (Sec 3.1), such that we have information at, near, and away from the resonant frequencies. Filled markers correspond to pinned contact lines, and empty markers denote mobile contact lines. Triangular markers represent a dominant jetting mode, diamond markers correspond to a dominant spreading mode, and circular markers represent trials where the dominant mode is both jetting and spreading. Linear fits are provided and are in good agreement with Eq.(15).

Sloshiness $\mathcal{S}_{\mathrm{RMS}}$ increases with increasing $\alpha$, as demonstrated in **Fig.6** and **Fig.7**. Such an increase is intuitive, since for a fixed set of frequencies, one would expect a higher degree of sloshing and drop deformation for higher pulsation amplitudes. Resonant frequencies for Kapton and PTFE are 85 and 90 Hz, respectively (**Fig.3**). For both beams, $\mathcal{S}_{\mathrm{RMS}}$ is less noisy around these frequencies, as represented by a higher R-squared value. Further from resonance, the variability in $\mathcal{S}_{\mathrm{RMS}}$ for a fixed $\alpha$ increases, as observed in **Fig.6** and **Fig.7**. Additionally, resonance allows for much higher $\mathcal{S}_{\mathrm{RMS}}$ before ejection, so for both beams the lowest $\mathcal{S}_{\mathrm{RMS}}$ is $f = 140$ Hz. The use of Womersley number in drop-canteliever systems is not totaly unprecedented. Previously[40], a modified Womersley number, dubbed the Kauffman number, was used to predict the damping of sessile drops on the end of a cantilever beam in ring-down vibration

Since the bending stiffness $EI$ of the PTFE beam is much lower than that of Kapton, the structural dynamics of PTFE are less favorable for sloshing in comparison. Conversely, a hydrophobic surface allows for easier deformation of the drop. Such conflicting behavior of the PTFE beam with respect to affecting $\mathcal{S}_{\mathrm{RMS}}$ result in a lower $(\mathcal{S}_{\mathrm{RMS}})_{\mathrm{max}}$ for PTFE beams, but similar $\mathcal{S}_{\mathrm{RMS}}$ as Kapton beams for the same $\alpha$ across all frequencies, as shown in **Fig.6** and **Fig.7**. Because of the hydrophobicity of PTFE, we only observe pinned contact lines at very low amplitude vibrations ($\alpha < 3$). The exception to this trend is in $f = 140$ Hz, as seen in **Fig.6**f, where the drop is pinned for high $\alpha$ values. Further examination shows that in those trials, the liquid drop moves from its initial location as the shaker turns on and settles on a location which presumably contains a blemish on the surface, pinning the drop. Nevertheless, the surface of Kapton is hydrophobic, so we observe pinned contact lines across the entire range of tested $\alpha$. The contact line mobility conditions here are largely stochastic, with some degree of dependence on the wettability of surface, surface energy, contaminants or any surface blemishes.

There is no appreciable difference in pinned and unpinned contact lines on the data of **Fig.6** and **Fig.7**, which may seem counterintuitive. Intuition is regained by the sloshing heatmaps of individual trials, as shown in **Fig.8**. The heatmaps correspond to individual trials performed on a Kapton beam around $\alpha \simeq 6.1 - 6.6$, respectively. Trials with pinned contact lines facilitate a stronger jetting mode, as seen with a taller apex and more intense warm tones in **Fig.8**a. When the contact line is mobile, the drop is allowed to spread, thus losing more energy to contact line friction[40]. The energy loss causes a smaller apex and less intense jetting mode, with a more pronounced spreading mode, shown in **Fig.8**b. This alternating act between jetting and spreading for pinned and mobile contact lines results in an overall similar $\mathcal{S}_{\mathrm{RMS}}$.

The deformation patterns visible in the heatmaps of **Fig.8** and **Fig.9** can be interpreted in the context of the mode classification framework established for sessile drops on rigid substrates[28,29]. The jetting mode, characterized by vertical elongation of the drop dome with minimal lateral spreading, is morphologically consistent with odd-$k$ zonal modes (e.g., $[3, 0]$), which produce an asymmetric vertical distortion of the free surface. The spreading mode, in which the drop flattens laterally, resembles even-$k$ zonal modes (e.g., $[2, 0]$), which produce a symmetric lateral–vertical exchange. While a modal decomposition requires three-dimensional surface reconstruction, our heatmaps provide a spatially resolved experimental visualization of drop deformation that complements the frequency-based mode identification used in prior studies[29,31]. Our observation that pinned contact lines promote jetting while mobile contact lines promote spreading is consistent with the theoretical prediction that contact-line pinning suppresses even-$k$ modes and shifts the spectral ordering[28,30]. For pinned drops, the constraint at the contact line forces deformation energy into vertical (odd-$k$) modes, producing the taller apex seen in **Fig.8**a. When the contact line is free to move,

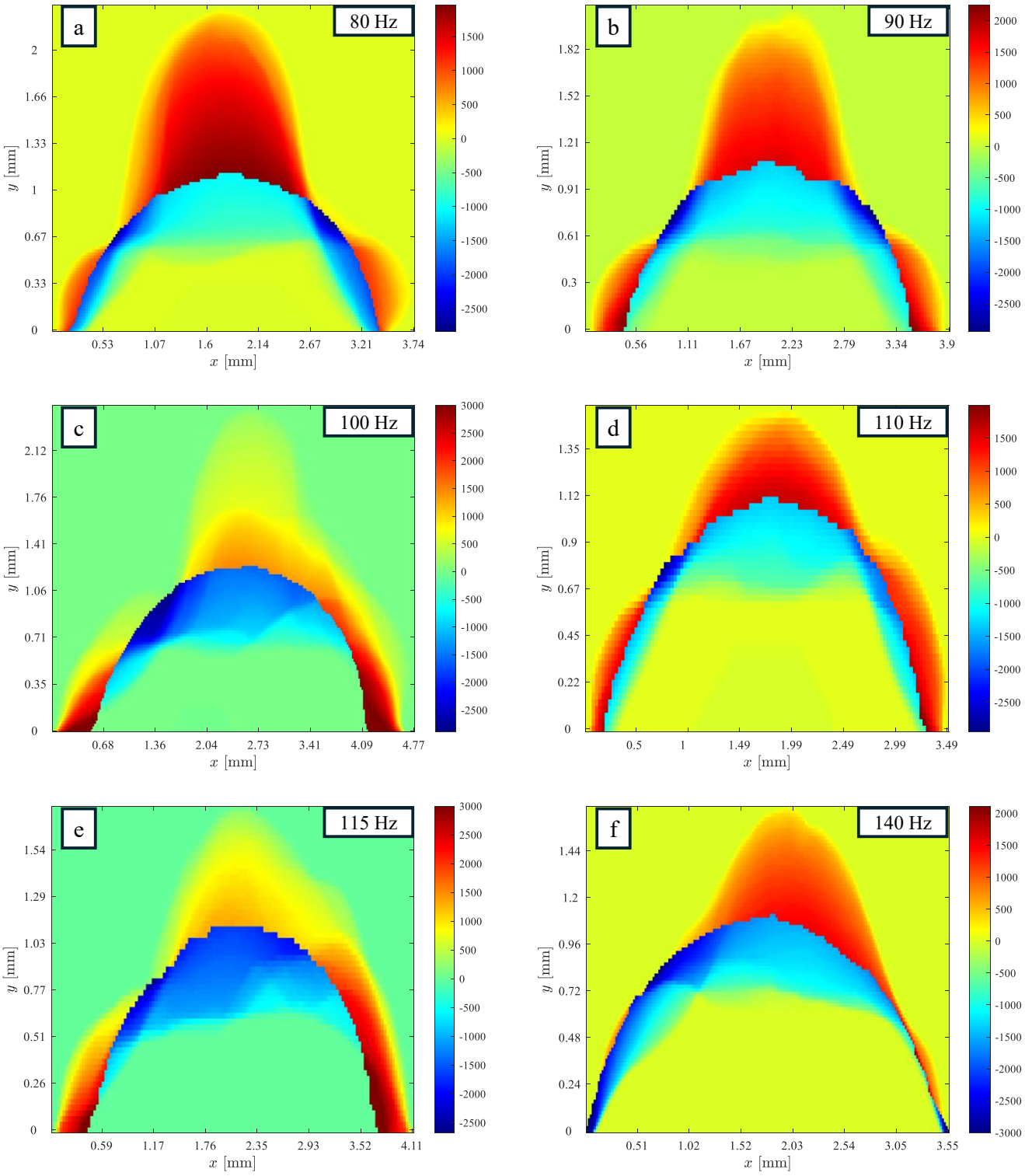



**Figure 8:** Drop heatmap with subtracted initial area for a sessile drop vibrating on a Kapton beam driven at $f =$ **(a)** 80, **(b)** 90, **(c)** 100, **(d)** 110, **(e)** 115, and **(f)** 140 Hz.

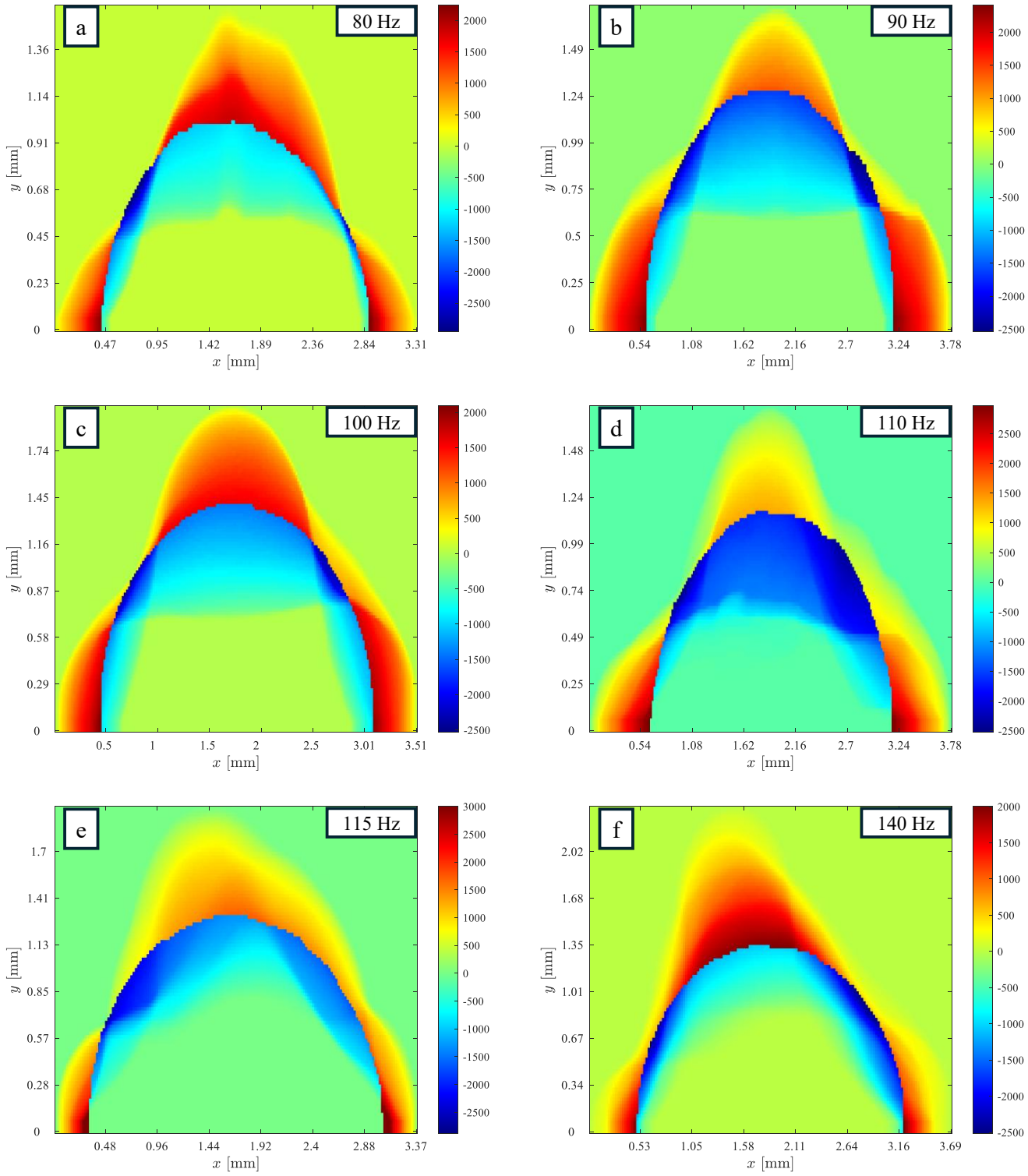



**Figure 9:** Drop heatmap with subtracted initial area for a sessile drop vibrating on a PTFE beam driven at $f =$ **(a)** 80, **(b)** 90, **(c)** 100, **(d)** 110, **(e)** 115, and **(f)** 140 Hz.

even-$k$ modes become accessible, and the drop can redistribute energy into lateral spreading, as observed in **Fig.8**b. Such contact-line-dependent mode selection is an additional source of dissipation beyond bulk viscosity[30].

# 4 Discussion and concluding remarks

In this study, we excite elastomeric cantilevers at various frequencies to describe how drops deposited on the end slosh. We describe the extent of drop deformation by a new parameter, sloshiness $\mathcal{S}$ a normalized projected area change from two orthogonal views. We find the natural frequency of our coupled system is lower than either of the uncoupled system frequencies in isolation. Drops augment the cantilever inertia by adding deflection due to increased inertia at the tip. A drop and cantilever beam oscillates with the same frequency for small initial deflections. We expand two-degree-of-freedom models, developed in the context of drop impact[16,39], to incorporate a harmonic oscillator driving the base to predict how sloshiness will change with base amplitude and frequency. The base oscillation we chose is purely harmonic, which makes the solution to Eq.(14) ill-conditioned and singular[41], and prevents us from finding unique values of $k_2$ and $c_2$. Modifications to the experiment to obtain the impulse or step response of the droplet while retaining a dominant frequency should resolve the singularity.

We emphasize that the 2-DOF model presented here is intentionally a reduced-order approximation. The complete theoretical framework for sessile drop oscillations[28,33] yields a rich modal spectrum that our lumped-parameter model does not resolve. However, our model serves to motivate the linear scaling $\mathcal{S} \sim \alpha$ by showing that the drop centroid displacement is proportional to the base displacement amplitude at steady state. With sufficient computational and experimental data, we believe this method could be used to quickly measure unknown liquid properties, viscosity, and surface tension, for very small volumes under low acceleration.

Though small drops deform less than large drops, their small deformation does not preclude their use as dampers. Liquid drops can be employed in low-acceleration vibration situations where particle impact dampers (PIDs) fail due to cessation of movement within the damper[40,42]. Drops experience no such decline in damping capacity, since even the smallest excitation can induce internal flow in the liquid continuum. Energy dissipation through internal flow and change in fluid boundaries makes liquid drops a good candidate for dampers without a lower bound for acceleration. Sloshiness as a parameter can thus be used to connect the change in fluid boundary to the damping capacity of a liquid drop in low acceleration environments.

The ability to remove resting drops from surfaces without external chemical or mechanical intervention is highly advantageous for hard-to-reach surfaces, ensuring cleanliness. Our work provides a foundation by which to adapt self-decontamination strategies to surfaces vulnerable to droplets, such as those in food preparation and healthcare, with a goal towards contaminant removal through harnessing surface properties and periodic excitation. We propose sloshiness as an analog to the energy expenditure inside deforming drops, shedding new light on the relationship between drop sloshing and ejection. Drop heatmaps show that pinned drops prefer jetting which resembles normal-to-substrate ejection, whereas mobile drops prefer spreading, which resembles the pinch-off or sliding ejection modes[8]. Future work can explore the relationship between different sloshing behavior and their corresponding ejection modes. Drop ejection modes are dependent on the substrate and the inertial force applied to the drop[8]. For highly damped beams like PTFE, we observe sloshiness plateauing before ejection at high acceleration. Tuning drop and surface parameters to induce desired sloshing and ejection behavior can be a fruitful objective for future researchers.

# 5 Data access

Raw experimental .mat files are publicly available in perpetuity via on Zenodo at 10.5281/zenodo.19576585.

# 6 Acknowledgement

We would like to thank the National Science Foundation (CBET-2346686, 2346687) for support.

# References


[1] Orkweha, P., Downing, A., Lebanoff, A. P., Zehtabian, S., Bacanli, S. S., Turgut, D. & Dickerson, A. K., 2021 Ensemble machine learning predicts displacement of cantilevered fibers impacted by falling drops. *Journal of Fluids and Structures* **102**, 103253.

[2] Worthington, A. M., 1877 XXVIII. On the forms assumed by drops of liquids falling vertically on a horizontal plate. *Proceedings of the royal society of London* **25**, 261–272.

[3] Rein, M., 1993 Phenomena of liquid drop impact on solid and liquid surfaces. *Fluid Dynamics Research* **12**, 61–93. ISSN 0169-5983. (doi:10.1016/0169-5983(93)90106-K).

[4] Yarin, A., 2006 DROP IMPACT DYNAMICS: Splashing, spreading, receding, bouncing.... *Annual Review of Fluid Mechanics* **38**, 159–192. ISSN 1545-4479. (doi:10.1146/annurev.fluid.38.050304.092144).

[5] Josserand, C. & Thoroddsen, S., 2016 Drop impact on a solid surface. *Annual Review of Fluid Mechanics* **48**, 365–391. ISSN 1545-4479. (doi:10.1146/annurev-fluid-122414-034401).

[6] Rioboo, R., Marengo, M. & Tropea, C., 2002 Time evolution of liquid drop impact onto solid, dry surfaces. *Experiments in Fluids* **33**, 112–124. ISSN 1432-1114. (doi:10.1007/s00348-002-0431-x).

[7] Erfanul Alam, M. & Dickerson, A. K., 2021 Sessile liquid drops damp vibrating structures. *Physics of Fluids* **33**, 062113. ISSN 1070-6631, 1089-7666. (doi:10.1063/5.0055382).

[8] Alam, M. E., Kauffman, J. L. & Dickerson, A. K., 2020 Drop ejection from vibrating damped, dampened wings. *Soft matter* **16**, 1931–194. ISSN 1744-683X. (doi:10.1039/c9sm02253h).

[9] Wang, F. & Fang, T., 2018 Post-impact drop vibration on a hydrophilic surface. *Experimental thermal and fluid science* **98**, 420–428. ISSN 0894-1777.

[10] Upadhyay, G., Kumar, V. & Bhardwaj, R. Bouncing droplets on an elastic, superhydrophobic cantilever beam **33**. ISSN 1070-6631. (doi:10.1063/5.0047868).

[11] Kumar, B., Upadhyay, G. & Bhardwaj, R., 2023 Coupled Dynamics of Droplet Impact on a Flexible, Hydrophilic Cantilever Beam. *Langmuir* **39**, 18768–18783. ISSN 0743-7463. (doi:10.1021/acs.langmuir.3c02238).

[12] Huang, X., Dong, X., Li, J. & Liu, J., 2019 Droplet impact induced large deflection of a cantilever. *Physics of Fluids* **31**, 062106. ISSN 1070-6631. (doi:10.1063/1.5099344).

[13] Shin, Y.-S. & Lim, H.-C., 2014 Shape oscillation and detachment conditions for a droplet on a vibrating flat surface. *The European Physical Journal E* **37**, 74. ISSN 1292-895X. (doi:10.1140/epje/i2014-14074-5).

[14] Fang, W., Wang, S., Duan, H., Tahir, S. A., Zhang, K., Wang, L., Feng, X.-Q. & Song, M., 2023 Target slinging of droplets with a flexible cantilever. *Droplet* **2**, n/a–n/a. ISSN 2731-4375. (doi:10.1002/dro2.72).

[15] Sharp, J. S., 2011 Resonant properties of sessile droplets; contact angle dependence of the resonant frequency and width in glycerol/water mixtures. *Soft Matter* **8**, 399–407. ISSN 1744-6848. (doi:10.1039/C1SM06916K).

[16] Fowler, C., Marshall, R., Son, M. & Jung, S., 2024 Resonance and damping in drop-cantilever interactions. *Physical Review Fluids* **9**, 123605. (doi:10.1103/PhysRevFluids.9.123605).

[17] Alam, M. E., Wu, D. & Dickerson, A. K., 2020 Predictive modelling of drop ejection from damped, dampened wings by machine learning. *Proceedings of the Royal Society A* **476**, 20200467.

[18] Brunet, P., Baudoin, M., Matar, O. B. & Zoueshtiagh, F., 2010 Droplet displacements and oscillations induced by ultrasonic surface acoustic waves: A quantitative study. *Physical Review E: Statistical Physics, Plasmas, Fluids, and Related Interdisciplinary Topics* **81**, 036315. (doi:10.1103/PhysRevE.81.036315).

[19] Snoeijer, J. H. & Andreotti, B., 2013 Moving contact lines: Scales, regimes, and dynamical transitions. *Annual Review of Fluid Mechanics* **45**, 269–292. ISSN 1545-4479. (doi:10.1146/annurev-fluid-011212-140734).

[20] Dong, L., Chaudhury, A. & Chaudhury, M. K., 2006 Lateral vibration of a water drop and its motion on a vibrating surface. *The European Physical Journal E* **21**, 231–242. ISSN 1292-895X. (doi:10.1140/epje/i2006-10063-7).

[21] Brunet, P., Eggers, J. & Deegan, R. D., 2007 Vibration-induced climbing of drops. *Physical Review Letters* **99**, 144501. (doi:10.1103/PhysRevLett.99.144501).

[22] Noblin, X., Buguin, A. & Brochard-Wyart, F., 2004 Vibrated sessile drops: Transition between pinned and mobile contact line oscillations. *The European Physical Journal E* **14**, 395–404. ISSN 1292-895X. (doi:10.1140/epje/i2004-10021-5).

[23] James, A. J., Vukasinovic, B., Smith, M. K. & Glezer, A., 2003 Vibration-induced drop atomization and bursting. *Journal of Fluid Mechanics* **476**, 1–28. (doi:10.1017/S0022112002002835).

[24] Ding, H., Gilani, M. N. H. & Spelt, P. D. M., 2010 Sliding, pinch-off and detachment of a droplet on a wall in shear flow. *Journal of Fluid Mechanics* **644**, 217–244. (doi:10.1017/S0022112009992217).

[25] Semprebon, C. & Brinkmann, M., 2014 On the onset of motion of sliding drops. *Soft Matter* **10**, 3325–3334. ISSN 1744-6848. (doi:10.1039/C3SM51959G).

[26] Vukasinovic, B., Smith, M. K. & Glezer, A., 2007 Dynamics of a sessile drop in forced vibration. *Journal of Fluid Mechanics* **587**, 395–423.

[27] Chang, C.-T., Bostwick, J. B., Steen, P. H. & Daniel, S., 2013 Substrate constraint modifies the Rayleigh spectrum of vibrating sessile drops. *Physical Review E* **88**, 023015. (doi:10.1103/PhysRevE.88.023015).

[28] Bostwick, J. B. & Steen, P. H., 2014 Dynamics of sessile drops. Part 1. Inviscid theory. *Journal of Fluid Mechanics* **760**, 5–38. (doi:10.1017/jfm.2014.582).

[29] Chang, C.-T., Bostwick, J. B., Daniel, S. & Steen, P. H., 2015 Dynamics of sessile drops. Part 2. Experiment. *Journal of Fluid Mechanics* **768**, 442–467. (doi:10.1017/jfm.2015.99).

[30] Bostwick, J. B. & Steen, P. H., 2016 Response of driven sessile drops with contact-line dissipation. *Soft Matter* **12**, 8919–8926. (doi:10.1039/C6SM01928E).

[31] Ding, D. & Bostwick, J. B., 2022 Pressure modes of the oscillating sessile drop. *Journal of Fluid Mechanics* **944**, R1. (doi:10.1017/jfm.2022.507).

[32] Zhang, F., Zhou, X. & Ding, H., 2023 Effects of gravity on natural oscillations of sessile drops. *Journal of Fluid Mechanics* **962**, A10. (doi:10.1017/jfm.2023.243).

[33] Bostwick, J. B. & Steen, P. H., 2015 Stability of constrained capillary surfaces. *Annual Review of Fluid Mechanics* **47**, 539–568. (doi:10.1146/annurev-fluid-010814-013626).

[34] Steen, P. H., Chang, C.-T. & Bostwick, J. B., 2019 Droplet motions fill a periodic table. *Proceedings of the National Academy of Sciences* **116**, 4849–4854. (doi:10.1073/pnas.1817065116).

[35] Dorbolo, S., Terwagne, D., Vandewalle, N. & Gilet, T., 2008 Resonant and rolling droplet. *New Journal of Physics* **10**, 113021. (doi:10.1088/1367-2630/10/11/113021).

[36] WU, J.-S. & CHEN, D.-W. Dynamic analysis of a uniform cantilever beam carrying a number of elastically mounted point masses with dampers **229**, 549–578. ISSN 0022-460X. (doi:10.1006/jsvi.1999.2504).

[37] Siddiqui, S. A. Q., Golnaraghi, M. F. & Heppler, G. R. Dynamics of a Flexible Cantilever Beam Carrying a Moving Mass **15**, 137–154. ISSN 1573-269X. (doi:10.1023/A:1008205904691).

[38] Gürgöze, M. On the eigenfrequencies of a cantilever beam with attached tip mass and a spring-mass system **190**, 149–162. ISSN 0022-460X. (doi:10.1006/jsvi.1996.0053).

[39] Gart, S., Mates, J. E., Megaridis, C. M. & Jung, S., 2015 Droplet Impacting a Cantilever: A Leaf-Raindrop System. *Physical review applied* **3**. ISSN 2331-7019. (doi:10.1103/PhysRevApplied.3.044019).

[40] Erfanul Alam, M. & Dickerson, A. K., 2021 Sessile liquid drops damp vibrating structures. *Physics of Fluids* **33**, 062113.

[41] Modarres-Sadeghi, Y., 2021 *Vibrations of One and Two Degree-of-Freedom Systems*, pp. 23–50. Cham: Springer International Publishing. ISBN 978-3-030-85884-1. (doi:10.1007/978-3-030-85884-1_3).

[42] Mao, K., Wang, M. Y., Xu, Z. & Chen, T., 2004 Simulation and characterization of particle damping in transient vibrations. *Journal of Vibration and Acoustics* **126**, 202–211. ISSN 1048-9002. (doi:10.1115/1.1687401).

[43] Ding, D., Sayyari, M. & Bostwick, J., 2024 Parametric oscillations of the sessile drop. *Journal of Fluid Mechanics* **995**, A3.